Supplementary Information: Mean-field theory of random close packings of axisymmetric particles

Adrian Baule[1,2], Romain Mari[1], Lin Bo[1], Louis Portal[1] & Hernán A. Makse[1]
[1]*Levich Institute and Physics Department, City College of New York, New York, New York 10031, USA*
[2]*School of Mathematical Sciences, Queen Mary University of London, London E1 4NS, UK*

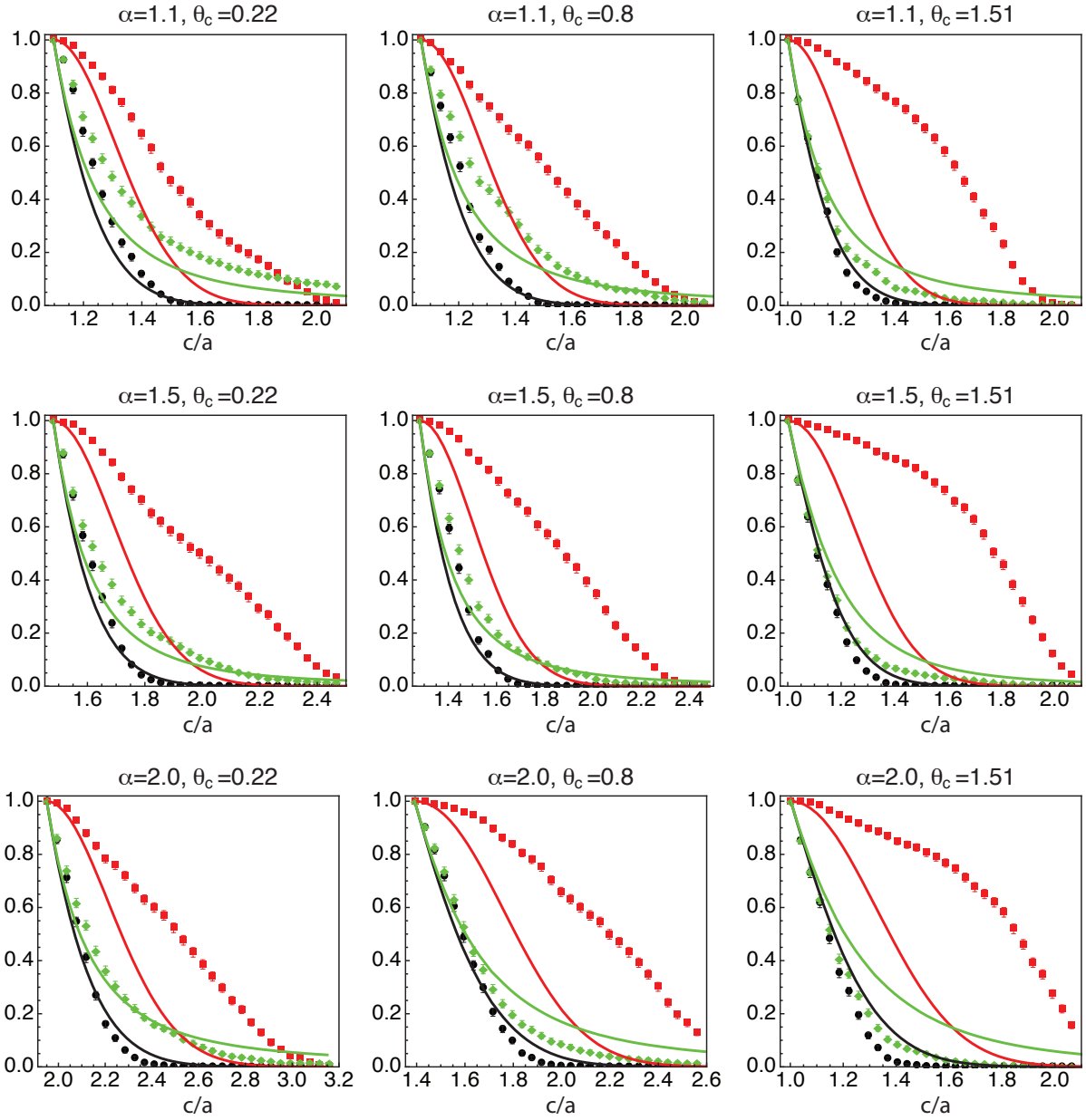

Supplementary Figure S1: **The plots of Fig. 7 shown on a linear scale.** We plot the theoretical predictions (solid lines) for $P(\mathbf{c}, z)$ (black), $P_{\mathrm{B}}(\mathbf{c})$ (red), and $P_{\mathrm{C}}(\mathbf{c}, z)$ (green) with the corresponding CDFs sampled from simulated configurations (symbols) of spherocylinders. For each aspect ratio $\alpha = 1.1, 1.5, 2.0$ we plot results for three values of the polar angle $\theta_{\mathrm{c}} \in [0, \pi/2]$. We generally observe that the three CDFs agree quite well in the regime of small c values, which provides the dominant contribution to the average Voronoi volume $\overline{W}(z)$. The error bars denote the root mean square error of the finite-size sampling.

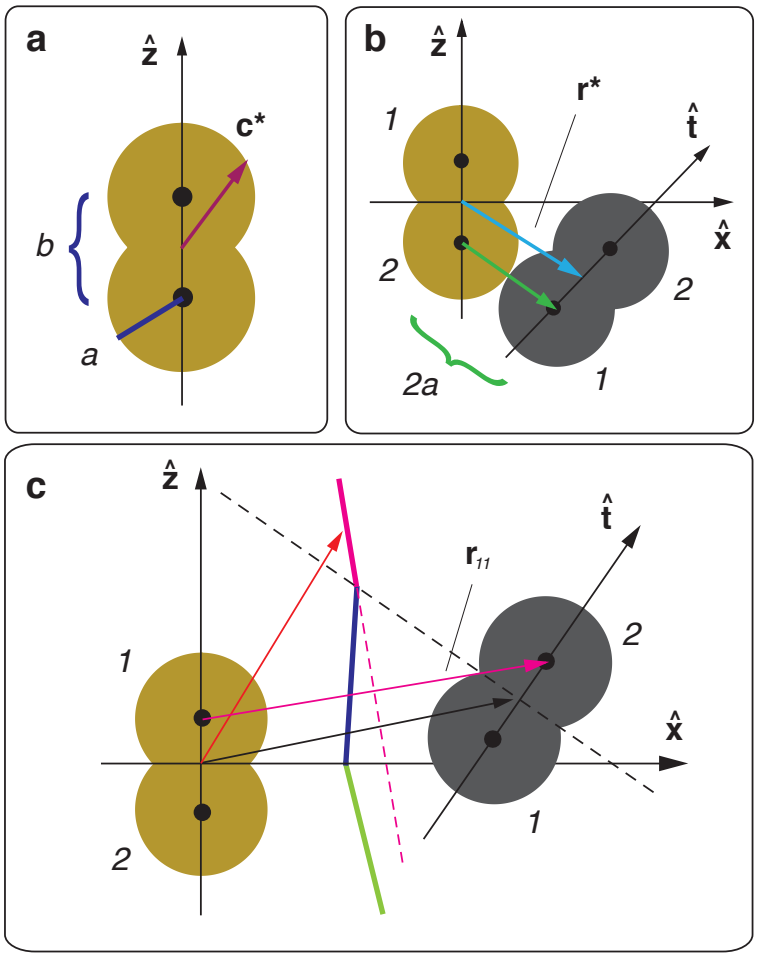

Supplementary Figure S2: **Parametrization of dimers. (a)** A dimer with parameters a and b. The hard core boundary is parametrized by the vector $\mathbf{c}^* = c^*(\theta_c)\hat{\mathbf{c}}$. **(b)**, The contact radius $r^*(\hat{\mathbf{r}}, \hat{\mathbf{t}})$ (light blue) is determined by the condition of contact between sphere 2 on the ith particle and 2 on the jth: $r^* = r^*_{22}$, where r^*_{22} is given by Eq. (S16). **(c)** The VB between two dimers of relative orientation $\hat{\mathbf{t}}$ and position $\mathbf{r}$. The VB is determined by the interactions between the different point pairs (indicated in different colors), which are separated following our algorithm in Fig. 3a. The pink part of the VB, e.g., is the VB between points 1 and 1, and is given by Eq. (S7).

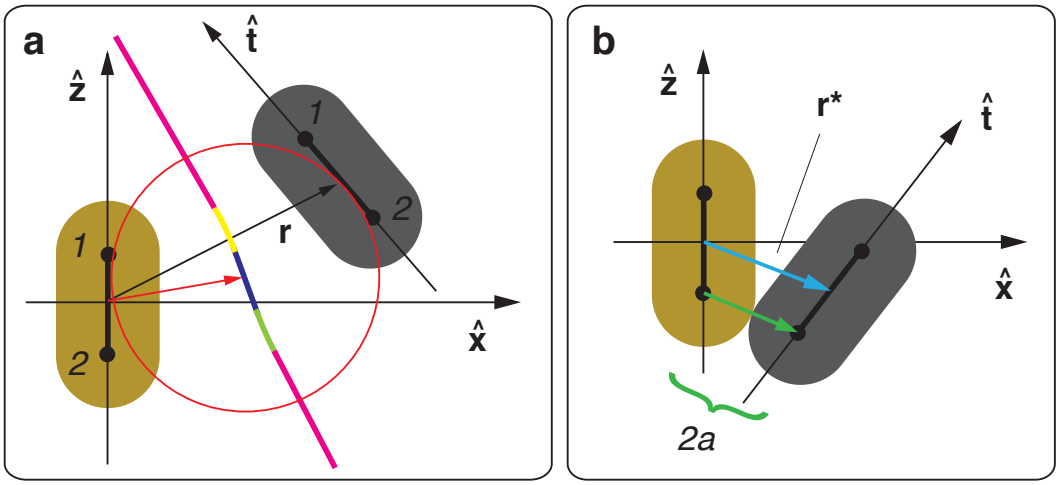

Supplementary Figure S3: **Parametrization of spherocylinders.** **(a)** The VB between two spherocylinders of relative orientation $\hat{\mathbf{t}}$ and position $\mathbf{r}$. The VB consists of the VBs due to the interaction of the four points and two lines (indicated in different colors), which are separated following our algorithm in Fig. 3a. The blue part of the VB, e.g., is due to the line-line interaction given by Eq. (S27): a sphere centered on this part touches the rods i and j for a unique radius. **(b)** The contact radius $r^*(\hat{\mathbf{r}}, \hat{\mathbf{t}})$ for two spherocylinders. Here, the contact is due to the spherical endcaps.

Shape	M_z	M_b	M_v
spherocylinder	2.767	1/2	3/2
dimer	3.60	1/2	3/2
prolate ellipsoid	4.833	1/3	1
oblate ellipsoid	-5.167	1/3	1

Supplementary Table S1: **Values of the shape-dependent constants in the analytic continuation of RCP**. Note that the M_z values for dimers and spherocylinders are taken from Fig. 6a in the main text, and the ones for the two rotationally symmetric ellipsoids from Ref. [6]. Due to the limited data, M_z is determined by linear interpolation.

Supplementary Note 1

In our simulation, we treat the case of spherocylinders. The interaction force between two particles is described as a linear function of the overlap. To obtain a jammed configuration, we follow previously studied protocols [22]. We start our simulation with a number of particles N, and generate particle positions randomly within a cubic box with size L and periodic boundary conditions. We first compress the initial system by shrinking the box size L to reach a certain pressure (which is very high at the first step, $P = 10^6$) and then let it relax fast until it fails to jam. We then compress the system and relax repeatedly several times until the system ends up in a stable but overcompressed configuration. This means that the pressure limit and relaxation rate we choose are too high to get to the jamming point. Thus we lower the pressure limit and relax the system slowly to obtain a less overcompressed configuration. We tune the two parameters, pressure and relaxation rate, until the system reaches a well jammed configuration with a very low pressure ($P < 10$). This procedure brings the system to the jamming point with minimal overlap.

Supplementary Methods

Calculation of the Voronoi boundary and the contact radius for dimers and spherocylinders

The Voronoi boundary (VB) between two objects is defined as the hypersurface that contains all the points that are equidistant to both objects. As before, we set the centre of our coordinate system to the centre of mass of particle i and fix the orientation of this particle along $\hat{\mathbf{z}}$. Given a direction $\hat{\mathbf{c}}$, a point on the VB is found at $s\hat{\mathbf{c}}$, where s depends on the position $\mathbf{r}$ and orientation $\hat{\mathbf{t}}$ of particle j: $s = s(\mathbf{r}, \hat{\mathbf{t}}, \hat{\mathbf{c}})$. The value of s is obtained from two conditions:

1. The point $s\hat{\mathbf{c}}$ has the minimal distance to each of the two objects along the direction $\hat{\mathbf{c}}$.
2. Both distances are the same.

The VB between two spheres of equal radii is the same as the VB between two points at the centres of the spheres. Therefore, condition 1 is trivially satisfied for every s and condition 2 translates into the equation

$$(s\hat{\mathbf{c}})^2 = (s\hat{\mathbf{c}} - \mathbf{r})^2, \tag{S1}$$

leading to

$$s = \frac{r}{2\hat{\mathbf{c}}\hat{\mathbf{r}}}, \tag{S2}$$

i.e., the VB is the plane perpendicular to the separation vector $\mathbf{r}$ at half the separation (see Fig. 2a, main text). Already for two spheres of unequal radii, the VB is a curved surface. Taking into account the different radii a_i and a_j, Eq. (S1) becomes

$$s - a_i = \sqrt{(s\hat{\mathbf{c}} - \mathbf{r})^2} - a_j, \tag{S3}$$

which has the solution

$$s = \frac{1}{2}\frac{r^2 - (a_i - a_j)^2}{\hat{\mathbf{c}}\hat{\mathbf{r}} - (a_i - a_j)}. \tag{S4}$$

Finding a solution for both conditions for general non-spherical objects is non-trivial. As discussed in the main part of the paper, from these two building blocks the VB between arbitrarily shaped objects can be constructed following our algorithm in Fig. 3 of the main text. For shapes consisting of a dense overlap of equal spheres like spherocylinders, this approach can be simplified by introducing a line interaction: The VB between two spherocylinders is equivalent to the VB between two lines at the centre of the cylindrical part. We first discuss the VB between two dimers, which represents the next simplest shape after a sphere.

Dimers

A dimer consists of two overlapping spheres and is defined by two parameters: the sphere radius a and the separation of the two sphere centres b (Supplementary Fig. S2a). The aspect ratio is then $\alpha = 1 + b/(2a)$. Due to the rotational symmetry, the hard core boundary $c^*(\hat{\mathbf{c}})$ of a dimer is parameterized by the polar angle θ_c only

$$c^*(\hat{\mathbf{c}}) = c^*(\theta_c) = a\left(\tilde{\alpha}|\cos(\theta_c)| + \sqrt{1 - \tilde{\alpha}\sin(\theta_c)}\right), \tag{S5}$$

where $\tilde{\alpha} = \alpha - 1 = b/(2a)$.

The VB between two dimers is generated by four different point interactions, which lead to four different values of the VB for a given direction $\hat{\mathbf{c}}$. In order to determine each of the four VBs in our coordinate system, we need the separation vectors for the four different point pairs. These are

$$\begin{aligned} \mathbf{r}_{11} &= \mathbf{r} - \tfrac{b}{2}(\hat{\mathbf{t}} + \hat{\mathbf{z}}), & \mathbf{r}_{12} &= \mathbf{r} + \tfrac{b}{2}(\hat{\mathbf{t}} - \hat{\mathbf{z}}), \\ \mathbf{r}_{21} &= \mathbf{r} - \tfrac{b}{2}(\hat{\mathbf{t}} - \hat{\mathbf{z}}), & \mathbf{r}_{22} &= \mathbf{r} + \tfrac{b}{2}(\hat{\mathbf{t}} + \hat{\mathbf{z}}), \end{aligned} \tag{S6}$$

where the subscript 11 denotes the top point on the ith dimer and the top point on the jth dimer. The VB $s\hat{\mathbf{c}}_{11} = s_{11}\hat{\mathbf{c}}$ due to the interaction between points 1 of i and 1 of j is then determined from the condition (Supplementary Fig. S2c)

$$\left(s_{11}\hat{\mathbf{c}} - \frac{b}{2}\hat{\mathbf{z}}\right)\hat{\mathbf{r}}_{11} = \frac{r_{11}}{2}. \tag{S7}$$

Likewise, for $s_{12}\hat{\mathbf{c}}$, $s_{21}\hat{\mathbf{c}}$, and $s_{22}\hat{\mathbf{c}}$. This leads to the four values

$$\begin{aligned} s_{11} &= \tfrac{r_{11}}{2\hat{\mathbf{c}}\hat{\mathbf{r}}_{11}} + \tfrac{b}{2}\tfrac{\hat{\mathbf{z}}\hat{\mathbf{r}}_{11}}{\hat{\mathbf{c}}\hat{\mathbf{r}}_{11}}, & s_{12} &= \tfrac{r_{12}}{2\hat{\mathbf{c}}\hat{\mathbf{r}}_{12}} + \tfrac{b}{2}\tfrac{\hat{\mathbf{z}}\hat{\mathbf{r}}_{12}}{\hat{\mathbf{c}}\hat{\mathbf{r}}_{12}}, \\ s_{21} &= \tfrac{r_{21}}{2\hat{\mathbf{c}}\hat{\mathbf{r}}_{21}} - \tfrac{b}{2}\tfrac{\hat{\mathbf{z}}\hat{\mathbf{r}}_{21}}{\hat{\mathbf{c}}\hat{\mathbf{r}}_{21}}, & s_{22} &= \tfrac{r_{22}}{2\hat{\mathbf{c}}\hat{\mathbf{r}}_{22}} - \tfrac{b}{2}\tfrac{\hat{\mathbf{z}}\hat{\mathbf{r}}_{22}}{\hat{\mathbf{c}}\hat{\mathbf{r}}_{22}}. \end{aligned} \tag{S8}$$

The VB between the two dimers is then given by s_{11}, if the point $s_{11}\hat{\mathbf{c}}$ is inside the appropriate region outlined by the separation lines in Fig. 3a in the main text. This is the case if

$$s_{11}\hat{\mathbf{c}}\hat{\mathbf{z}} > 0, \qquad \text{and} \qquad \hat{\mathbf{t}}(s_{11}\hat{\mathbf{c}} - \mathbf{r}) > 0. \tag{S9}$$

For s_{12} the conditions are

$$s_{12}\hat{\mathbf{c}}\hat{\mathbf{z}} > 0, \qquad \text{and} \qquad \hat{\mathbf{t}}(s_{12}\hat{\mathbf{c}} - \mathbf{r}) < 0, \tag{S10}$$

and likewise for s_{21}, and s_{22}

$$s_{21}\hat{\mathbf{c}}\hat{\mathbf{z}} < 0, \qquad \text{and} \qquad \hat{\mathbf{t}}(s_{12}\hat{\mathbf{c}} - \mathbf{r}) > 0, \tag{S11}$$

$$s_{22}\hat{\mathbf{c}}\hat{\mathbf{z}} < 0, \qquad \text{and} \qquad \hat{\mathbf{t}}(s_{12}\hat{\mathbf{c}} - \mathbf{r}) < 0. \tag{S12}$$

This yields a unique value s for the VB along $\hat{\mathbf{c}}$, so that overall the VB consists of a union of at most four different flat surfaces depending on the relative orientation and position of the two dimers.

Contact radius

In order to calculate the excluded volume and surface, V^* and S^*, respectively, we require the contact radius $r^*(\hat{\mathbf{r}}, \hat{\mathbf{t}})$, which is the value of r for which a dimer j with orientation $\hat{\mathbf{t}}$ and solid angle $\hat{\mathbf{r}}$ is in contact with dimer i. Two equal spheres are in contact, when their separation is twice the radius. For two dimers, there are thus four different conditions for contact: $r_{11} = 2a$ and likewise for r_{12}, r_{21}, and r_{22}. Solving these four condition for r using the Eqs. (S6), yields the value of r for contact of sphere 1 of i and sphere 1 of j, which we denote by r^*_{ij} (Supplementary Fig. S2b):

$$r^*_{11}(\hat{\mathbf{r}}, \hat{\mathbf{t}}) = \frac{b}{2}\left(\hat{\mathbf{r}}\hat{\mathbf{t}} + \hat{\mathbf{r}}\hat{\mathbf{z}} + \sqrt{(\hat{\mathbf{r}}\hat{\mathbf{t}} + \hat{\mathbf{r}}\hat{\mathbf{z}})^2 + \frac{4}{\tilde{\alpha}^2} - 2(1 + \hat{\mathbf{t}}\hat{\mathbf{z}})}\right). \tag{S13}$$

Likewise,

$$r^*_{12}(\hat{\mathbf{r}}, \hat{\mathbf{t}}) = \frac{b}{2}\left(-\hat{\mathbf{r}}\hat{\mathbf{t}} + \hat{\mathbf{r}}\hat{\mathbf{z}} + \sqrt{(\hat{\mathbf{r}}\hat{\mathbf{t}} - \hat{\mathbf{r}}\hat{\mathbf{z}})^2 + \frac{4}{\tilde{\alpha}^2} - 2(1 - \hat{\mathbf{t}}\hat{\mathbf{z}})}\right), \tag{S14}$$

$$r^*_{21}(\hat{\mathbf{r}}, \hat{\mathbf{t}}) = \frac{b}{2}\left(\hat{\mathbf{r}}\hat{\mathbf{t}} - \hat{\mathbf{r}}\hat{\mathbf{z}} + \sqrt{(\hat{\mathbf{r}}\hat{\mathbf{t}} - \hat{\mathbf{r}}\hat{\mathbf{z}})^2 + \frac{4}{\tilde{\alpha}^2} - 2(1 - \hat{\mathbf{t}}\hat{\mathbf{z}})}\right), \tag{S15}$$

$$r^*_{22}(\hat{\mathbf{r}}, \hat{\mathbf{t}}) = \frac{b}{2}\left(-(\hat{\mathbf{r}}\hat{\mathbf{t}} + \hat{\mathbf{r}}\hat{\mathbf{z}}) + \sqrt{(\hat{\mathbf{r}}\hat{\mathbf{t}} + \hat{\mathbf{r}}\hat{\mathbf{z}})^2 + \frac{4}{\tilde{\alpha}^2} - 2(1 + \hat{\mathbf{t}}\hat{\mathbf{z}})}\right). \tag{S16}$$

The correct overall r^* is then the maximum of the r^*_{ij}. This follows simply if we imagine a configuration with fixed relative orientation $\hat{\mathbf{t}}$ and angular position $\hat{\mathbf{r}}$. For a large radius r the two dimers are not in contact. Now decrease r. The correct contact radius is then the largest value of r for which the two dimers are in contact for the first time, since for any of the smaller r^* there might be overlap.

Spherocylinders

A spherocylinder consists of a cylindrical part of length L and radius a, with two semi-spheres of radius a as endcaps (Supplementary Fig. S3b). This yields the aspect ratio $\alpha = 1 + L/(2a)$. As for dimers, the hard core boundary of a spherocylinder is parameterized only by the polar angle θ_c due to the rotational symmetry

$$c^*(\theta_c) = a \begin{cases} \tilde{\alpha}\left(\cos(\theta_c) + \sqrt{\frac{1}{\tilde{\alpha}^2} - \sin^2(\theta_c)}\right), & 0 \le \theta_c < \arctan(\tilde{\alpha}^{-1}) \\ \sin(\theta_c)^{-1}, & \arctan(\tilde{\alpha}^{-1}) \le \theta_c \le \pi/2, \end{cases} \tag{S17}$$

where $\tilde{\alpha} = \alpha - 1 = L/(2a)$.

The VB between two spherocylinders is identical to the VB between the line segments at the centre of the cylindrical part. In the following we refer to these line segments as "rods". As before, we align rod i with the $\hat{\mathbf{z}}$ axis of our coordinate system, so that a point on it is parameterized by the vector $t_i\hat{\mathbf{z}}$ with $t_i \in [-L/2; L/2]$. Likewise, the orientation of rod j is given by $\hat{\mathbf{t}}$, so that a point on rod j is parameterized by $\mathbf{r} + t_j\hat{\mathbf{t}}$, where also $t_j \in [-L/2; L/2]$.

We solve the two conditions that define the VB as follows. The square of the distance between $s\hat{\mathbf{c}}$ and a point on rod i is

$$D_i^2 = (t_i\hat{\mathbf{z}} - s\hat{\mathbf{c}})^2, \tag{S18}$$

and likewise the distance between $s\hat{\mathbf{c}}$ and a point on rod j

$$D_j^2 = (\mathbf{r} + t_j\hat{\mathbf{t}} - s\hat{\mathbf{c}})^2. \tag{S19}$$

Condition 1. then requires:

$$\frac{\partial D_i^2}{\partial t_i} = 0, \tag{S20}$$

$$\frac{\partial D_j^2}{\partial t_j} = 0. \tag{S21}$$

This leads to the minimal values

$$t_i^{\min} = s\hat{\mathbf{c}}\hat{\mathbf{z}} = s(\hat{\mathbf{c}}\hat{\mathbf{z}}), \tag{S22}$$

$$t_j^{\min} = (s\hat{\mathbf{c}} - \mathbf{r})\hat{\mathbf{t}} = s(\hat{\mathbf{c}}\hat{\mathbf{t}}) - r. \tag{S23}$$

Condition 2. requires:

$$D_i^{\min} = D_j^{\min}, \tag{S24}$$

which leads to

$$(t_i^{\min}\hat{\mathbf{z}} - s\hat{\mathbf{c}})^2 = (t_j^{\min}\hat{\mathbf{t}} + \mathbf{r} - s\hat{\mathbf{c}})^2. \tag{S25}$$

Eq. (S25) does not take into account that the rods have a finite length L, so that t_i^{min} and t_j^{min} are only the correct minimal values when $t_i^{\min} \in [-L/2, L/2]$ and $t_j^{\min} \in [-L/2, L/2]$. We refer to this case as a *line-line* interaction between the two rods. If t_i^{min} and/or t_j^{min} are not $\in [-L/2, L/2]$ interactions involving the end-points of the rods arise. Overall, one has to distinguish the cases:

1. *Line-line* interaction: $t_i^{\min} \in [-L/2, L/2]$ and $t_j^{\min} \in [-L/2, L/2]$ (1 case).
2. *Line-point* interaction between the segment i and an end-point of j: $t_i^{\min} \in [-L/2, L/2]$ and $t_j = \pm L/2$ (2 cases).
3. *Point-line* interaction between the segment j and an end-point of i: $t_j^{\min} \in [-L/2, L/2]$ and $t_i = \pm L/2$ (2 cases).
4. *Point-point* interaction between the end points of i and j: $t_i = \pm L/2$ and $t_j = \pm L/2$ (4 cases).

In the following we use different subscripts in order to refer to the different Voronoi interactions, e.g., s_{ll} for line-line interaction, s_{lp} for a line-point interaction, etc. The separation of the different interactions follows the algorithm outlined in Fig. 3b in the main text. Note that the four point-point interactions are flat surfaces, while interactions involving the line segment are curved.

Line-line interaction

This case arises if t_i^{min} and t_j^{min} fall inside the length of the segments. The conditions are thus:

$$t_i^{\min} \in [-L/2, L/2], \qquad t_j^{\min} \in [-L/2, L/2]. \tag{S26}$$

In this case t_i^{min} and t_j^{min} are given by Eqs. (S22) and (S23). Substituting these expressions into Eq. (S25) then leads to a quadratic equation for the value $s = s_{\rm ll}$ of the boundary:

$$\frac{s_{\rm ll}^2}{r^2}\Big[(\hat{\mathbf{c}}\hat{\mathbf{z}})^2 - (\hat{\mathbf{c}}\hat{\mathbf{t}})^2\Big] + 2\frac{s_{\rm ll}}{r}\Big[(\hat{\mathbf{c}}\hat{\mathbf{t}})(\hat{\mathbf{r}}\hat{\mathbf{t}}) - \hat{\mathbf{r}}\hat{\mathbf{c}}\Big] + 1 - (\hat{\mathbf{r}}\hat{\mathbf{t}})^2 = 0. \tag{S27}$$

The correct solution of this equation is the real and positive one. Clearly, the line-line Voronoi boundary between the two rods scales with the separation r.

Eqs. (S26) are satisfied when

$$-L/2 \le s_{\rm ll}\hat{\mathbf{c}}\hat{\mathbf{z}} \le L/2, \quad \text{and} \quad -L/2 \le (s_{\rm ll}\hat{\mathbf{c}} - \mathbf{r})\hat{\mathbf{t}} \le L/2, \tag{S28}$$

which defines the separation lines for the line interactions on each of the two spherocylinders in Fig. 3b. The VB due to the line-line interaction is illustrated further in the Supplementary Fig. S3a: A sphere centred at the VB touches both rods i and j for a unique radius.

Line-point interaction

In this case $t_i^{\min}$ falls along the line segment i and $t_j^{\min}$ is at one of the end points of rod j. We choose the top of $\mathbf{t}_j$ as the point, indicated by a subscript 1 and we obtain:

$$t_i^{\min} \in [-L/2, L/2], \qquad t_j^{\min} = L/2. \tag{S29}$$

Substituting the Eq. (S22) for t_i^{min} and $t_j^{\min} = L/2$ into Eq. (S25) then leads to a quadratic equation for $s = s_{\rm lp_1}$, where the index p_1 refers to the top point:

$$\frac{s_{\rm lp_1}^2}{r^2}(\hat{\mathbf{c}}\hat{\mathbf{z}})^2 - 2\frac{s_{\rm lp_1}}{r}\Big[(\hat{\mathbf{r}}\hat{\mathbf{c}}) + \frac{L}{2r}(\hat{\mathbf{c}}\hat{\mathbf{t}})\Big] + \left(\frac{L}{2r}\right)^2 + \frac{L}{r}(\hat{\mathbf{r}}\hat{\mathbf{t}}) + 1 = 0. \tag{S30}$$

The corresponding expression for the Voronoi boundary with respect to the bottom point $s_{\rm lp_2}$, where $t_j^{\min} = -L/2$, simply follows by setting $L \to -L$ in Eq. (S30). The conditions for the two line-point interactions are then

$$-L/2 \le s_{\rm lp_1}\hat{\mathbf{c}}\hat{\mathbf{z}} \le L/2 \qquad \text{and} \qquad (s_{\rm lp_1}\hat{\mathbf{c}} - \mathbf{r})\hat{\mathbf{t}} \ge L/2 \tag{S31}$$

$$-L/2 \le s_{\rm lp_2}\hat{\mathbf{c}}\hat{\mathbf{z}} \le L/2 \qquad \text{and} \qquad (s_{\rm lp_2}\hat{\mathbf{c}} - \mathbf{r})\hat{\mathbf{t}} \le -L/2. \tag{S32}$$

Point-line interaction

This interaction is analogous to line-point. The conditions are:

$$t_i^{\min} = L/2, \qquad t_j^{\min} \in [-L/2, L/2]. \tag{S33}$$

Substituting $t_i^{\min} = L/2$ for the top point and Eq. (S23) into Eq. (S25) leads to

$$\begin{aligned}&\frac{s_{\rm p_1l}^2}{r^2}(\hat{\mathbf{c}}\hat{\mathbf{t}})^2 + 2\frac{s_{\rm p_1l}}{r}[(\hat{\mathbf{r}}\hat{\mathbf{c}}) - (\hat{\mathbf{c}}\hat{\mathbf{t}})(\hat{\mathbf{r}}\hat{\mathbf{t}})]\\ &-\frac{s_{\rm p_1l}}{r}\frac{L}{r}(\hat{\mathbf{c}}\hat{\mathbf{z}}) + \left(\frac{L}{2r}\right)^2 + (\hat{\mathbf{r}}\hat{\mathbf{t}})^2 - 1 = 0.\end{aligned} \tag{S34}$$

Likewise for $s_{\rm p_2l}$. The conditions for the two point-line interactions are then

$$s_{\rm p_1l}\hat{\mathbf{c}}\hat{\mathbf{z}} \ge L/2, \qquad \text{and} \qquad -L/2 \le (s_{\rm p_1l}\hat{\mathbf{c}} - \mathbf{r})\hat{\mathbf{t}} \le L/2 \tag{S35}$$

$$s_{\rm p_2l}\hat{\mathbf{c}}\hat{\mathbf{z}} \le -L/2, \qquad \text{and} \qquad -L/2 \le (s_{\rm p_2l}\hat{\mathbf{c}} - \mathbf{r})\hat{\mathbf{t}} \le L/2. \tag{S36}$$

Point-point interaction

In this case the two points $t_i^{\min}$ and $t_j^{\min}$ are both fixed and equal to $L/2$ or $-L/2$. Writing

$$t_i^{\min} = L_i/2, \qquad t_j^{\min} = L_j/2, \tag{S37}$$

where $L_i = \pm L$ and $L_j = \pm L$ for the top and bottom points on each of the rods, we find for the solution of Eq. (S25) with Eqs. (S37):

$$s_{pp} = r\,\frac{1 + \frac{L_j}{r}(\hat{\mathbf{r}}\hat{\mathbf{t}})}{2(\hat{\mathbf{r}}\hat{\mathbf{c}}) + \frac{L_j}{r}(\hat{\mathbf{c}}\hat{\mathbf{t}}) - \frac{L_i}{r}(\hat{\mathbf{c}}\hat{\mathbf{z}})}. \tag{S38}$$

Here, the interactions for, e.g., the two top points $s_{\mathrm{p_1p_1}}$ is obtained by setting $L_i = L_j = L$. Likewise for the other point interactions. The conditions for the four different point-point Voronoi boundaries are then

$$s_{\mathrm{p_1p_1}}\hat{\mathbf{c}}\hat{\mathbf{z}} \geq L/2, \quad \text{and} \quad (s_{\mathrm{p_1p_1}}\hat{\mathbf{c}} - \mathbf{r})\hat{\mathbf{t}} \geq L/2, \tag{S39}$$

$$s_{\mathrm{p_1p_2}}\hat{\mathbf{c}}\hat{\mathbf{z}} \geq L/2, \quad \text{and} \quad (s_{\mathrm{p_1p_2}}\hat{\mathbf{c}} - \mathbf{r})\hat{\mathbf{t}} \leq -L/2, \tag{S40}$$

$$s_{\mathrm{p_2p_1}}\hat{\mathbf{c}}\hat{\mathbf{z}} \leq -L/2, \quad \text{and} \quad (s_{\mathrm{p_2p_1}}\hat{\mathbf{c}} - \mathbf{r})\hat{\mathbf{t}} \geq L/2, \tag{S41}$$

$$s_{\mathrm{p_2p_2}}\hat{\mathbf{c}}\hat{\mathbf{z}} \leq -L/2, \quad \text{and} \quad (s_{\mathrm{p_2p_2}}\hat{\mathbf{c}} - \mathbf{r})\hat{\mathbf{t}} \leq -L/2. \tag{S42}$$

In the limit $L/r \to 0$, we recover from Eq. (S38) the Voronoi boundary between two equal spheres, Eq. (S2).

Contact radius

In order to determine the contact radius $r^*(\hat{\mathbf{r}}, \hat{\mathbf{t}})$ of two spherocylinders, one has to distinguish the possible contacts of the spherical endcaps and of the cylindrical segments. As before, we denote a point on rod i by $t_i\hat{\mathbf{z}}$ and a point on rod j by $\mathbf{r} + t_j\hat{\mathbf{t}}$. The squared distance between these two points is

$$\begin{aligned} D^2(\mathbf{r}, \hat{\mathbf{t}}, t_i, t_j) &= (t_i\hat{\mathbf{z}} - (\mathbf{r} + t_j\hat{\mathbf{t}}))^2 \\ &= t_i^2 + t_j^2 + r^2 + 2r(t_j(\hat{\mathbf{r}}\hat{\mathbf{t}}) - t_i(\hat{\mathbf{r}}\hat{\mathbf{z}})) - 2t_it_j(\hat{\mathbf{z}}\hat{\mathbf{t}}). \end{aligned} \tag{S43}$$

The two spherocylinders are in contact when the minimum of D^2 with respect to t_i and t_j, i.e., the minimal squared separation, is the square of the diameter $(2a)^2$. Solving $\partial D^2/\partial t_i = 0$ and $\partial D^2/\partial t_j = 0$ yields the two minimal positions

$$t_i^* = r\frac{(\hat{\mathbf{r}}\hat{\mathbf{z}}) - (\hat{\mathbf{r}}\hat{\mathbf{t}})(\hat{\mathbf{z}}\hat{\mathbf{t}})}{1 - (\hat{\mathbf{z}}\hat{\mathbf{t}})^2} = rA_i \tag{S44}$$

$$t_j^* = r\frac{(\hat{\mathbf{r}}\hat{\mathbf{z}})(\hat{\mathbf{z}}\hat{\mathbf{t}}) - (\hat{\mathbf{r}}\hat{\mathbf{t}})}{1 - (\hat{\mathbf{z}}\hat{\mathbf{t}})^2} = rA_j, \tag{S45}$$

which define A_i and A_j. Substituting these expressions into Eq. (S43) and solving for r under the condition $D^2 = 4a^2$ yields the contact radius

$$r_{\mathrm{ll}}^*(\hat{\mathbf{r}}, \hat{\mathbf{t}}) = \frac{2a}{\sqrt{1 + (A_i\hat{\mathbf{z}} - A_j\hat{\mathbf{t}})^2 + 2(A_j(\hat{\mathbf{r}}\hat{\mathbf{t}}) - A_i(\hat{\mathbf{r}}\hat{\mathbf{z}}))}}. \tag{S46}$$

This contact radius does not take into account the finite length of the spherocylinders and is only valid for $t_i^* \in [-L/2, L/2]$ and $t_j^* \in [-L/2, L/2]$. In fact, r_{ll}^* is the contact between the line segments (indicated by the subscript as before). As for the different Voronoi interactions one has to distinguish further the line-point, point-line and line-line contacts in addition to the line-line one (Supplementary Fig. S3b).

For the line-point contact one has to consider $t_j = \pm L/2$, so one has to solve

$$\frac{\partial}{\partial t_i} D^2\left(\mathbf{r}, \hat{\mathbf{t}}, t_i, \pm\frac{L}{2}\right) = 0 \tag{S47}$$

to find the minimal $t_i^{*\mathrm{lp}}$. Substituting this value back into D^2 and solving $D^2 = 4a^2$ for r yields the two line-point contact radii, which are valid when $t_i^{*\mathrm{lp}} \in [-L/2, L/2]$. For the point-line contact one has to consider $t_i = \pm L/2$, so that the corresponding equation is given by

$$\frac{\partial}{\partial t_j} D^2\left(\mathbf{r}, \hat{\mathbf{t}}, \pm\frac{L}{2}, t_j\right) = 0 \tag{S48}$$

determines the minimal $t_j^{*\mathrm{pl}}$. Substituting this value back into D^2 and solving $D^2 = 4a^2$ for r yields the two point-line contact radii. These are valid when $t_j^{*\mathrm{pl}} \in [-L/2, L/2]$. For the point-point contact one can solve directly

$$D^2\left(\mathbf{r}, \hat{\mathbf{t}}, \pm\frac{L}{2}, \pm\frac{L}{2}\right) = 4a^2 \tag{S49}$$

for r, which yields four different point-point contact radii.

Overall, one thus obtains 9 possible different valid values for the contact radius $r^*(\hat{\mathbf{r}}, \hat{\mathbf{t}})$, similar to the different Voronoi interactions. The unique correct radius is then the maximum of all positive and real ones.

Calculation of the packing fraction

Here, we summarize our method to calculate the packing fraction of dimers and spherocylinders, shown in Fig. 6b in the main text. We first calculate V^* and S^* numerically for a range of $\mathbf{c}$ values. The excluded volume is defined as $V^* = \langle \Omega - \Omega \cap V_{\mathrm{ex}} \rangle_{\hat{\mathbf{t}}}$, which can be expressed as an orientational average over a volume integral:

$$V^*(\mathbf{c}) \;=\; \left\langle \int \mathrm{d}\mathbf{r}\, \Theta(r - r^*(\hat{\mathbf{r}}, \hat{\mathbf{t}}))\Theta(c - s(\mathbf{r}, \hat{\mathbf{t}}, \hat{\mathbf{c}}))\Theta(s(\mathbf{r}, \hat{\mathbf{t}}, \hat{\mathbf{c}})) \right\rangle_{\hat{\mathbf{t}}}. \tag{S50}$$

We parametrize these integrals in spherical coordinates and denote with θ_r, the polar angle of the position and with β_r the azimuthal angle of the position. The corresponding orientational angles have a subscript t. Eq. (S50) can then be written in terms of the multi-dimensional integral

$$V^*(c, \theta_{\mathrm{c}}) \;=\; \frac{1}{2\pi} \int_0^{\pi} \mathrm{d}\theta_r \int_{-\pi}^{\pi} \mathrm{d}\beta_r \int_0^{\pi/2} \mathrm{d}\theta_t \int_{-\pi}^{\pi} \mathrm{d}\beta_t \int_{r^*(\theta_r,\beta_r,\theta_t,\beta_t)}^{\infty} \mathrm{d}r\, r^2 \sin(\theta_t)\sin(\theta_r)\Theta[c - s(r, \theta_r, \beta_r, \theta_t, \beta_t, \theta_{\mathrm{c}})]\Theta[s(r, \theta_r, \beta_r, \theta_t, \beta_t, \theta_{\mathrm{c}})]. \tag{S51}$$

Here, the integration limits of the θ_t integration only take distinct orientations into account. Eq. (S51) is a five dimensional integral, which we calculate numerically using a Monte-Carlo method for a given $\mathbf{c}$.

The excluded surface is defined $S^* = \langle \partial V_{\mathrm{ex}} \cap \Omega \rangle_{\hat{\mathbf{t}}}$, which can be expressed as an orientational average over a surface integral:

$$S^*(\mathbf{c}) \;=\; \left\langle \oint \mathrm{d}\hat{\mathbf{r}}\, \Theta(c - s(\mathbf{r}, \hat{\mathbf{t}}, \hat{\mathbf{c}}))\Theta(s(\mathbf{r}, \hat{\mathbf{t}}, \hat{\mathbf{c}}))\Big|_{r=r^*(\hat{\mathbf{r}},\hat{\mathbf{t}})} \right\rangle_{\hat{\mathbf{t}}}, \tag{S52}$$

Here, one has to take into account the surface element for a non-constant radius $r^*(\hat{\mathbf{r}}, \hat{\mathbf{t}})$. Using the same parametrization as for the excluded volume, the surface element can be calculated and yields

$$\mathrm{d}\hat{\mathbf{r}} = r^* \sqrt{\left(r^{*2} + \left(\frac{\partial r^*}{\partial \theta_r}\right)^2\right)\sin^2(\theta_r) + \left(\frac{\partial r^*}{\partial \beta_r}\right)^2}\, \mathrm{d}\theta_r \mathrm{d}\beta_r, \tag{S53}$$

which recovers the usual surface element $\mathrm{d}\hat{\mathbf{r}} = r^{*2}\sin(\theta_r)\mathrm{d}\theta_r\mathrm{d}\beta_r$ for $r^* = \text{const}$. Eq. (S52) can thus be written in terms of the multi-dimensional integral

$$\begin{aligned} S^*(c, \theta_{\mathrm{c}}) \;=\; & \frac{1}{2\pi} \int_0^{\pi} \mathrm{d}\theta_r \int_{-\pi}^{\pi} \mathrm{d}\beta_r \int_0^{\pi/2} \mathrm{d}\theta_t \int_{-\pi}^{\pi} \mathrm{d}\beta_t \sin(\theta_t) r^* \sqrt{\left(r^{*2} + \left(\frac{\partial r^*}{\partial \theta_r}\right)^2\right)\sin^2(\theta_r) + \left(\frac{\partial r^*}{\partial \beta_r}\right)^2} \\ & \times\Theta[c - s(r^*, \theta_r, \beta_r, \theta_t, \beta_t, \theta_{\mathrm{c}})]\Theta[s(r^*, \theta_r, \beta_r, \theta_t, \beta_t, \theta_{\mathrm{c}})], \end{aligned} \tag{S54}$$

where $r^* = r^*(\theta_r, \beta_r, \theta_t, \beta_t)$. Eq. (S54) can also be computed numerically using Monte-Carlo for a given $\mathbf{c}$.

In the next step we determine the surface density $\sigma(z)$ with the method outlined in the section Methods: We generate local configurations of z contacting particles and determine the probability density function $p_\mathrm{m}(c_\mathrm{m}, \hat{\mathbf{c}})$ of the minimal VB along a direction $\hat{\mathbf{c}}$. This yields the average

$$\langle S^*(c_\mathrm{m}, \hat{\mathbf{c}})\rangle = \int_{c^*}^{\infty} S^*(y, \hat{\mathbf{c}}) p_\mathrm{m}(y, \hat{\mathbf{c}}) \mathrm{d}y, \tag{S55}$$

and the surface density follows via Eq. (12) for integer values of z

$$\sigma(z) = \frac{1}{\langle\langle S^*(c_\mathrm{m}, \hat{\mathbf{c}})\rangle\rangle_{\hat{\mathbf{c}}}}.$$

The average Voronoi volume can then be calculated by solving the self-consistent equation (4) numerically for a given integer z. The volume integral on the right hand side of Eq. (4) with Eq. (8) reads explicitly for the rotationally symmetric dimers and spherocylinders

$$\overline{W}(z) \;=\; V_\alpha + 4\pi \int_0^{\pi/2} \mathrm{d}\theta_c \sin(\theta_\mathrm{c}) \int_{c^*(\theta_\mathrm{c})}^{\infty} \mathrm{d}c\, c^2 \exp\left\{-\frac{V^*(c, \theta_\mathrm{c})}{\overline{W}(z) - V_\alpha} - \sigma(z)\, S^*(c, \theta_\mathrm{c})\right\}. \tag{S56}$$

In order to solve this equation numerically we calculate the two-dimensional integral on the right hand side using our numerically obtained V^*, S^*, and $\sigma(z)$ for a given z over a range of $\overline{W} = x$ values. This yields a function $G(x)$. The average Voronoi volume $\overline{W}$ is then the value of x that satisfies $G(x) = x$ and the packing fraction $\phi(z, \alpha)$ follows as $V_\alpha/\overline{W}$. For fractional z that are predicted from our evaluation of degenerate configurations (Methods), we use a linear interpolation to obtain $\phi(z(\alpha), \alpha)$.

Analytic continuation of the spherical random close packing

Close to the spherical point, the self-consistent Eq. (4) can be solved analytically and allows the calculation of an analytic continuation from the RCP point. The key is to introduce suitable approximations of V^* and S^* for α close to 1. We assume that, as the particles are deformed from the sphere, the change in the excluded volume and surface terms is dominated by the hard-core exclusion, while the change due to the Voronoi interaction can be neglected. This means that V^* and S^* are given by the spherical excluded volume and surface, but shifted by $c^*(\hat{\mathbf{c}}) - a$:

$$V^*(\mathbf{c}) \;=\; V_1^*(c - (c^*(\hat{\mathbf{c}}) - a)), \tag{S57}$$

$$S^*(\mathbf{c}) \;=\; S_1^*(c - (c^*(\hat{\mathbf{c}}) - a)). \tag{S58}$$

Here, V_1^* and S_1^* are the corresponding expressions for spheres [22]:

$$V_1^*(c) \;=\; V_1\left(\left(\frac{c}{a}\right)^3 - 4 + 3\frac{a}{c}\right), \tag{S59}$$

$$S_1^*(c) \;=\; 2S_1\left(1 - \frac{a}{c}\right), \tag{S60}$$

with V_1 and S_1 denoting the volume and surface of a sphere with radius a. In the following, the subscript 1 always refers to quantities in spherical packings with $\alpha = 1$. With these approximations, the self-consistent Eq. (4) becomes

$$\overline{W} \;=\; V_\alpha + \oint \mathrm{d}\hat{\mathbf{c}} \int_{c^*(\hat{\mathbf{c}})}^{\infty} \mathrm{d}c\, c^2 \exp\left\{-\frac{1}{\overline{W} - V_\alpha} V_1^*(c - (c^*(\hat{\mathbf{c}}) - a)) - \sigma(z) S_1^*(c - (c^*(\hat{\mathbf{c}}) - a))\right\}. \tag{S61}$$

We transform the integration variable into

$$x = \frac{c - (c^*(\hat{\mathbf{c}}) - a)}{a}. \tag{S62}$$

Substituting into Eq. (S61) the expressions for V_1^* and S_1^*, Eqs. (S59) and (S60), and dividing the equation by the sphere volume V_1 leads to

$$\omega \;=\; \frac{3}{4\pi} \oint \mathrm{d}\hat{\mathbf{c}} \int_1^{\infty} \mathrm{d}x \left(x + \frac{c^*(\hat{\mathbf{c}})}{a} - 1\right)^2 \exp\left\{-\frac{1}{\omega}\left(x^3 + \frac{3}{x} - 4\right) - \tilde{\sigma}(z)\left(1 - \frac{1}{x}\right)\right\}, \tag{S63}$$

where we define the quantities

$$\omega = \frac{\overline{W} - V_\alpha}{V_1}, \qquad \tilde{\sigma}(z) = 2S_1\sigma(z). \tag{S64}$$

Rearranging terms yields

$$\omega \;=\; 3\left\langle \int_1^\infty \mathrm{d}x \left(x + \frac{c^*(\hat{\mathbf{c}})}{a} - 1\right)^2 \exp\left\{-\frac{1}{\omega}\left(x^3 + (3 - \tilde{\sigma}(z)\omega)\,\frac{1}{x} - 4 - \tilde{\sigma}(z)\omega\right)\right\}\right\rangle_{\hat{\mathbf{c}}}. \tag{S65}$$

Now we use the identity

$$-\omega\frac{\mathrm{d}}{\mathrm{d}x}\exp\left\{-\frac{1}{\omega}\left(x^3 + (3 - \tilde{\sigma}(z)\omega)\,\frac{1}{x} - 4 - \tilde{\sigma}(z)\omega\right)\right\} \;=\; \left(3x^2 - (3 - \tilde{\sigma}(z)\omega)\,\frac{1}{x^2}\right)\exp\left\{-\frac{1}{\omega}\left(x^3 + (3 - \tilde{\sigma}(z)\omega)\,\frac{1}{x} - 4 - \tilde{\sigma}(z)\omega\right)\right\} \tag{S66}$$

to obtain from Eq. (S65)

$$0 \;=\; \left\langle \int_1^\infty \mathrm{d}x \left((3 - \tilde{\sigma}(z)\omega)\,\frac{1}{x^2} + 6x(c^*(\hat{\mathbf{c}})/a - 1) + 3(c^*(\hat{\mathbf{c}})/a - 1)^2\right)\exp\left\{-\frac{1}{\omega}\left(x^3 + (3 - \tilde{\sigma}(z)\omega)\,\frac{1}{x} - 4 - \tilde{\sigma}(z)\omega\right)\right\}\right\rangle_{\hat{\mathbf{c}}}. \tag{S67}$$

In the spherical limit $\alpha \to 1$, we have $c^* \to a$ and one can show that [22]

$$\tilde{\sigma}_1(z) = z\,\sqrt{3}/2. \tag{S68}$$

In this case Eq. (S67) becomes

$$0 \;=\; (3 - \tilde{\sigma}_1(z)\omega_1)\int_1^\infty \mathrm{d}x\,\frac{1}{x^2}\exp\left[-\frac{1}{\omega_1}\left(x^3 + (3 - \tilde{\sigma}_1(z)\omega_1)\,\frac{1}{x} - 4 - \tilde{\sigma}_1(z)\omega_1\right)\right], \tag{S69}$$

which has the exact solution

$$3 - \tilde{\sigma}_1(z)\omega_1 = 0, \tag{S70}$$

so that the free volume becomes

$$\omega_1(z) = \frac{3}{\tilde{\sigma}_1(z)} = \frac{2\sqrt{3}}{z}, \tag{S71}$$

using Eq. (S68). In order to solve Eq. (S67) for $\alpha \neq 1$, we approximate

$$e^{-(3-\tilde{\sigma}(z)\omega)\frac{1}{\omega x}} \approx 1 - (3 - \tilde{\sigma}(z)\omega)\,\frac{1}{\omega\,x}, \tag{S72}$$

which is an appropriate approximation since the dominant term in the exponent for the given integration limits is x^3 and $\tilde{\sigma}(z)$ is of order 1 for small aspect ratios. This leads to

$$0 \;=\; \left\langle \int_1^\infty \mathrm{d}x \left((3 - \tilde{\sigma}(z)\omega)\,\frac{1}{x^2} + 6x(c^*(\hat{\mathbf{c}})/a - 1) + 3(c^*(\hat{\mathbf{c}})/a - 1)^2\right)\left(1 - (3 - \tilde{\sigma}(z)\omega)\,\frac{1}{\omega\,x}\right)e^{-x^3/\omega}\right\rangle_{\hat{\mathbf{c}}}, \tag{S73}$$

so that the integration over x and the orientational average become independent. We obtain further

$$0 \;=\; \int_1^\infty \mathrm{d}x \left((3 - \tilde{\sigma}(z)\omega)\,\frac{1}{x^2} + 6x\,\langle(c^*(\hat{\mathbf{c}})/a - 1)\rangle_{\hat{\mathbf{c}}} + 3\left\langle(c^*(\hat{\mathbf{c}})/a - 1)^2\right\rangle_{\hat{\mathbf{c}}}\right)\left(\omega - (3 - \tilde{\sigma}(z)\omega)\,\frac{1}{x}\right)e^{-x^3/\omega}, \tag{S74}$$

or, after rewriting the integrals,

$$\begin{aligned} 0 \;=\; & -(3 - \tilde{\sigma}(z)\omega)^2\,f_{-3}(\omega) - (3 - \tilde{\sigma}(z)\omega)\left[6\,\langle(c^*(\hat{\mathbf{c}})/a - 1)\rangle_{\hat{\mathbf{c}}}\,f_0(\omega) + 3\left\langle(c^*(\hat{\mathbf{c}})/a - 1)^2\right\rangle_{\hat{\mathbf{c}}} f_{-1}(\omega) - \omega f_{-2}(\omega)\right] \\ & +6\omega\,\langle(c^*(\hat{\mathbf{c}})/a - 1)\rangle_{\hat{\mathbf{c}}}\,f_1(\omega) + 3\omega\left\langle(c^*(\hat{\mathbf{c}})/a - 1)^2\right\rangle_{\hat{\mathbf{c}}} f_0(\omega). \end{aligned} \tag{S75}$$

This equation is quadratic in $3 - \tilde{\sigma}(z)\omega$ and contains the basic integrals

$$f_n(y) = \int_1^\infty \mathrm{d}x\, x^n\, e^{-x^3/y}, \tag{S76}$$

which can not be expressed in closed form. The solution of Eq. (S75) is

$$3 - \tilde{\sigma}(z)\omega = F_\alpha(\omega), \tag{S77}$$

where we indicate the dependence on α explicitly. In the spherical limit, we have $F_1(\omega) = 0$ and we recover the spherical result. By expanding the function $F_\alpha(\omega)$ we therefore obtain an analytical continuation of the spherical solution. In the following we neglect quadratic terms in the deviation from the sphere. Expanding $F_\alpha(\omega)$ into a Taylor series up to linear orders in $\tilde{\alpha} = \alpha - 1$ leads to

$$3 - \tilde{\sigma}(z)\omega = -6M_\mathrm{b}h(\omega)\tilde{\alpha}, \tag{S78}$$

where

$$h(y) = \frac{f_1(y)}{f_{-2}(y)}, \tag{S79}$$

and the constant M_b denotes the relative first-order deviation of the object boundary from the sphere (the subscript b refers to "boundary"):

$$M_\mathrm{b} = \frac{1}{a}\,\frac{\mathrm{d}}{\mathrm{d}\alpha}\,\langle c^*(\hat{\mathbf{c}})\rangle_{\hat{\mathbf{c}}}\Big|_{\alpha=1}. \tag{S80}$$

We are interested in an analytic continuation of the spherical RCP point as the sphere is deformed. At RCP the coordination number is given by the isostatic value $\bar{z} = 6$, so that the free volume Eq. (S71) at RCP becomes $\bar{\omega}_1 = \omega_1(\bar{z}) = 1/\sqrt{3}$. If we expand $h(\omega)$ around $\bar{\omega}_1$ to linear orders in $\tilde{\alpha}$ we obtain from Eq. (S78)

$$3 - \tilde{\sigma}(z)\omega = -6M_\mathrm{b}(h(\bar{\omega}_1) + h'(\bar{\omega}_1))(\omega - \bar{\omega}_1)\tilde{\alpha}, \tag{S81}$$

which can be solved for ω

$$\omega = \frac{3 + 6M_\mathrm{b}(h(\bar{\omega}_1) - h'(\bar{\omega}_1)\bar{\omega}_1)\tilde{\alpha}}{\tilde{\sigma}(z) - 6M_\mathrm{b}h'(\bar{\omega}_1)\tilde{\alpha}}. \tag{S82}$$

By factoring out the spherical surface density at RCP, $\tilde{\sigma}_1(\bar{z})$, in the denominator and using $\bar{\omega}_1 = 3/\tilde{\sigma}_1(\bar{z})$ from Eq. (S71) we obtain further

$$\omega = \bar{\omega}_1 \frac{1 + 2M_\mathrm{b}(h(\bar{\omega}_1) - h'(\bar{\omega}_1)\bar{\omega}_1)\tilde{\alpha}}{\tilde{\sigma}(z)/\tilde{\sigma}_1(\bar{z}) - 2M_\mathrm{b}h'(\bar{\omega}_1)\bar{\omega}_1\tilde{\alpha}}. \tag{S83}$$

For simplicity in the notation, we introduce the two functions

$$g_1(y) = 2(h(y) - h'(y)y) \tag{S84}$$

$$g_2(y) = 2h'(y)y. \tag{S85}$$

We also multiply ω by V_1/V_α, which yields the reduced free volume per particle: $\omega_\alpha = \omega V_1/V_\alpha$. In turn, ω_α is directly related to the packing fraction due to Eq. (S64)

$$\phi = \frac{1}{1 + \omega_\alpha}. \tag{S86}$$

With Eq. (S83) we obtain for ω_α

$$\omega_\alpha = \bar{\omega}_1 \frac{1 + M_\mathrm{b}g_1(\bar{\omega}_1)\tilde{\alpha}}{\tilde{\sigma}(z)/\tilde{\sigma}_1(\bar{z}) - M_\mathrm{b}g_2(\bar{\omega}_1)\tilde{\alpha}}\,\frac{V_1}{V_\alpha}. \tag{S87}$$

The crucial step is then to find a suitable approximation for the surface density close to the spherical point. For spheres, the density is linear in z, Eq. (S68). Since z increases rapidly from the spherical point [32], we assume that the increase in the surface density is dominated by the increase in the coordination number. Consequently,

$$\frac{\tilde{\sigma}(z)}{\tilde{\sigma}_1(\bar{z})} \approx \frac{z(\alpha)}{\bar{z}} \approx 1 + M_z\tilde{\alpha}. \tag{S88}$$

In the last step, we have introduced the first-order deviation of the coordination number from the isostatic value

$$M_z = \frac{1}{\bar{z}} \frac{\mathrm{d}}{\mathrm{d}\alpha} z(\alpha)\bigg|_{\alpha=1}. \tag{S89}$$

Substituting Eq. (S88) into Eq. (S87) leads to our final result for the reduced free volume per particle

$$\omega_\alpha = \bar{\omega}_1 \frac{1 + M_\mathrm{b} g_1(\bar{\omega}_1)\tilde{\alpha}}{[1 + (M_z - M_\mathrm{b} g_2(\bar{\omega}_1))\tilde{\alpha}][1 + M_\mathrm{v}\tilde{\alpha}]}, \tag{S90}$$

where we use the first-order variation of the object volume

$$M_\mathrm{v} = \frac{1}{V_1} \frac{\mathrm{d}}{\mathrm{d}\alpha} V_\alpha\bigg|_{\alpha=1} = \frac{1}{V_1} \frac{\mathrm{d}}{\mathrm{d}\alpha} \left\langle c^*(\hat{\mathbf{c}})^3 \right\rangle_{\hat{\mathbf{c}}}\bigg|_{\alpha=1}. \tag{S91}$$

By expressing $\tilde{\alpha}$ in terms of z using Eq. (S88) one can also derive an exact expression for $\phi(z)$, namely Eq. (13) in the main text (with $\bar{\omega}_1 \to \omega_1$ for simplicity in the notation). At the isostatic value $z = \bar{z}$, Eq. (13) recovers the spherical RCP value $\phi(\bar{z}) = (1 + \bar{\omega}_1)^{-1}$. The inversion of Eq. (13) can be performed exactly by solving a quadratic equation for $z(\phi)$, leading to the analytic continuation of the spherical equation of state. For a considerable range of ϕ values, the resulting $z(\phi)$ curves are in excellent agreement with the solution obtained by numerically integrating the exact V^* and S^* for dimers and spherocylinders, as shown in Fig. 6c in the main text. Moreover, the maximal packing densities of dimers and spherocylinders from simulations lie very close to the predicted $z(\phi)$ continuation.

Note that Eq. (S90) will lead to different results for the continuation depending on the boundary parametrization $c^*(\hat{\mathbf{c}})$ used for the particular shape. For example, the parametrization Eq. (S17) for spherocylinders implies a linearly increasing object volume with $\tilde{\alpha}$: $V_\alpha = V_1(1 + 1.5\tilde{\alpha})$. Instead, one could use a parametrization that leaves the volume constant $V_\alpha = V_1$, by rescaling the radius a in Eq. (S17) by the factor $(1 + 1.5\tilde{\alpha})^{1/3}$, resulting in a different ω_α for the *same* aspect ratio. This is not a physical inconsistency of the theory, but originates in the approximations for V^* and S^* given by Eq. (S58), which are proportional to V_1 and S_1 and thus also depend on a. Rescaling only the radius of the spherocylinder, while leaving V_1 and S_1 unchanged, therefore gives rise to different approximations. In our approximation, the radii of V_1 and S_1 are both identical to the radius a of the spherical components of the dimers and spherocylinders for all aspect ratios, and thus V^* and S^* are locally given by the spherical excluded volume and surface.

Supplementary Table S1 summarizes the values of M_z, M_b, and M_v for the rotationally symmetric shapes dimers, spherocylinders, and prolate/oblate ellipsoids. The values of the remaining constants in Eq. (S90) are:

$$\bar{\omega}_1 = 1/\sqrt{3}, \qquad g_1(\bar{\omega}_1) = 2.177, \qquad g_2(\bar{\omega}_1) = 0.615. \tag{S92}$$

The resulting analytic continuations are plotted in the inset of Fig. 6c in the main text.

From Eq. (13) we derive a simple condition such that a given shape increases the packing density beyond RCP upon deformation. The condition $\phi'(\bar{z}) > 0$ leads to the inequality

$$\left[g_1(\bar{\omega}_1) + g_2(\bar{\omega}_1)\right] \frac{M_\mathrm{b}}{M_z} - \frac{M_\mathrm{v}}{M_z} < 1. \tag{S93}$$

For prolate shapes we have $M_z \geq 0$, so that Eq. (S93) is already satisfied if $\left[g_1(\omega_1) + g_2(\omega_1)\right] M_\mathrm{b} - M_\mathrm{v} < 0$, which is valid for dimers, spherocylinders, and prolate ellipsoids. A similar argument holds for oblate shapes, where $M_z \leq 0$.